2020 IEEE International Conference on Robotics and Automation (ICRA)
31 May - 31 August, 2020. Paris, France

Coordinate-Free Dynamics and Differential Flatness of a Class of 6DOF Aerial Manipulators

Jake Welde and Vijay Kumar

***Abstract*— In this work, we derive a coordinate-free formulation of the coupled dynamics of a class of 6DOF aerial manipulators consisting of an underactuated quadrotor equipped with a 2DOF articulated manipulator, and demonstrate that the system is differentially flat with respect to the end effector pose. In particular, we require the center of mass of the entire system to be fixed in the end effector frame, suggesting a reasonable mechanical design criterion. We make use of an inertial decoupling transformation to demonstrate differential flatness, allowing us to plan dynamically feasible trajectories for the system in the space of the 6DOF pose of the end effector, which is ideal for achieving precise manipulator tasks. Simulation results validate the flatness-based planning methodology for our dynamic model, and its usefulness is demonstrated in a simulated aerial videography task.**

I. Introduction

In recent years, micro aerial vehicles (MAVs) such as quadrotors have demonstrated exciting progress across a wide range of important fields from precision agriculture [1] to disaster response [2] and transporting medical products [3]. The agility, adaptability, payload capacity, and intelligence of these systems enable them to navigate in challenging environments while passively collecting actionable data, transporting static payloads, and avoiding undesired contact with obstacles. While these abilities show great promise for critical challenges faced by society, one of the greatest current limitations of MAVs as compared to mobile ground robots and fixed-based robots is their extreme limitations in physical interaction with the environment. Mobile ground robots are able to accomplish a wide range of useful physical tasks including dexterous teleoperation [4] and rolling transport of objects [5]. Fixed-base manipulator arms are able to complete precision pouring tasks [6] and continue to develop greater capabilities for manipulation in cluttered environments [7].

We wish to endow aerial robots with the same capacity to manipulate objects in their environment, while also allowing them to leverage their much greater workspace and agility. Significant challenges arise in the dynamic modeling, planning, and control of aerial manipulators. Without active compensation in the controller, the coupled dynamics of the *floating base* (in our case, a quadrotor) and the manipulator arm will cause instability or poor tracking performance for each subsystem [8]. When considering an underactuated floating base, the most common case for MAVs such as quadrotors today, an arbitrary disturbance wrench from the manipulator cannot be instantaneously countered, requiring the planning of dynamically feasible system trajectories that allow the base to counter these disturbances.

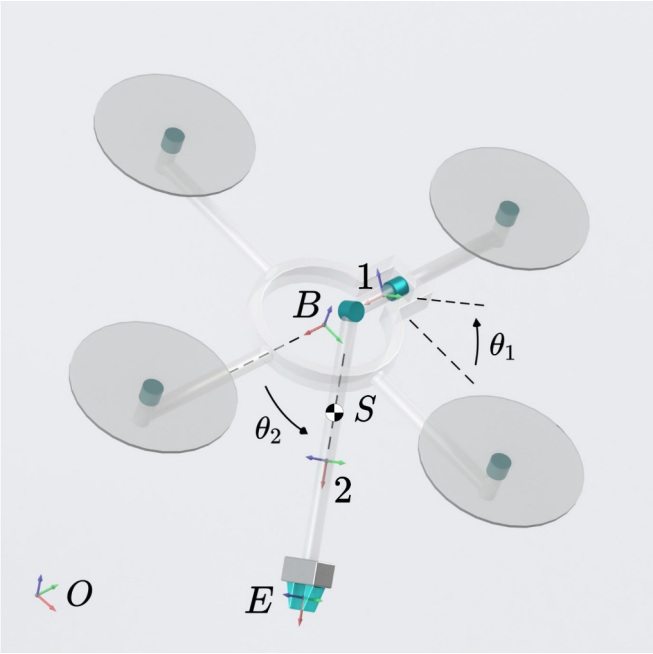

Fig. 1: Schematic representation of the aerial manipulator considered, consisting of an underactuated *floating base* B and two articulated links 1 and 2, both with nonzero inertia, with coordinate frames located at the center of mass of each body. The manipulator is designed such that the center of mass of the entire system S is fixed in the end effector frame E for all configurations. O is an inertial frame.

There has been extensive research in the area of aerial manipulation over the last decade [9]. Aerial manipulators have tackled problems ranging from inspection by contact [10] to high-speed payload acquisition [11], while unactuated *slung load* systems have been used to precisely transport payloads [12], [13]. However, prior work in aerial manipulation is subject to a number of assumptions and restrictions that limit its applicability to many practical circumstances, including:

The authors are with the General Robotics Automation Sensing and Perception (GRASP) Laboratory at the University of Pennsylvania, Philadelphia, PA 19104 USA. *emails:* {jwelde,kumar}@seas.upenn.edu. We gratefully acknowledge the support of ARL grant DCIST CRA W911NF-17-2-0181, NSF Grants CNS-1446592, and CNS-1521617, ARO grant W911NF-13-1-0350, Qualcomm Research, United Technologies, Intel Corporation, and C-BRIC, a Semiconductor Research Corporation Joint University Microelectronics Program cosponsored by DARPA. This material is based upon work supported by the National Science Foundation Graduate Research Fellowship under Grant No. DGE-1845298.

- The floating base is fully actuated [10] or has a 2D actuation force [14] (as compared to 1D for the quadrotor)
- The dynamics are formulated in 2D [11][15], or end effector trajectories are limited to the sagittal plane, preventing full 6DOF manipulation [16], [17]
- A method for planning trajectories in a physically useful space is absent [18], or criteria for dynamically feasible trajectories are not established [17]
- The dynamics are not explicitly derived [14], [17]–[20] or are derived using Euler Angles for the floating base attitude, introducing artificial singularities [21]–[25]
- Only the inertia of two rigid bodies is considered despite multiple DOF in the manipulator arm [19], [26]

In this work, we derive a coordinate-free dynamic model of a 3D aerial manipulator consisting of an underactuated floating base and a 2DOF articulated arm. The dynamics of the respective subsystems of the aerial manipulator are decoupled using a well-known principle involving the center of mass of the combined system. We then leverage this decomposition, along with our requirement that the system center of mass S be fixed in the end effector frame E, to demonstrate that the system is differentially flat with respect to the end effector pose. This allows us to determine the necessary control inputs to nominally track arbitary end effector trajectories in 6DOF, which is extremely useful for a wide range of manipulation tasks.

The rest of the paper is organized as follows. In Sec. II, we more formally define the system in question. In Sec III, we derive the singularity-free dynamics of the aerial manipulator. Sec. IV introduces a transformation of the dynamics that will be useful in planning and control. Sec. V demonstrates the differential flatness of the system and determines the required control inputs. Sec. VI applies the approach to a task in simulation. Sec. VII concludes the paper.

II. System Definition

The system consists of an underactuated floating base comprised by a quadrotor, equipped with a 2DOF manipulator arm, shown in Fig. 1. We establish coordinate frames at the center of mass of the floating base and two manipulator links, respectively called $B, 1$, and 2. We also establish an inertial coordinate frame O and the end effector frame E, parallel to 2.

The configuration our system $\boldsymbol{q} = \{\boldsymbol{g}_{OB}, \boldsymbol{\theta}\}$ lives on the 8-dimensional manifold $Q := \mathrm{SE}(3) \times \mathbb{R}^2$, where

$$\boldsymbol{g}_{OB} = \begin{bmatrix} \boldsymbol{R}_{OB} & \boldsymbol{p}_{OB} \\ 0 & 1 \end{bmatrix} \tag{1}$$

is the homogeneous transformation matrix from the floating base frame to the world frame, and $\boldsymbol{\theta}$ is the 2-tuple of joint angles, also known as shape coordinates. Our velocity vector is

$$\boldsymbol{v} = \begin{bmatrix} \boldsymbol{v}_{OB}^{\mathrm{T}} & \boldsymbol{\omega}_{OB}^{\mathrm{T}} & \dot{\boldsymbol{\theta}}^{\mathrm{T}} \end{bmatrix}^{\mathrm{T}} \in \mathbb{R}^8 \tag{2}$$

where $\boldsymbol{V}_{OB} = \begin{bmatrix} \boldsymbol{v}_{OB}^{\mathrm{T}} & \boldsymbol{\omega}_{OB}^{\mathrm{T}} \end{bmatrix}^{\mathrm{T}}$ is the twist of the floating base expressed the body frame B. The kinematics of the floating base therefore take the form

$$\dot{\boldsymbol{R}}_{OB} = \boldsymbol{R}_{OB}\hat{\boldsymbol{\omega}}_{OB} \tag{3}$$

$$\dot{\boldsymbol{p}}_{OB} = \boldsymbol{R}_{OB}\boldsymbol{v}_{OB} \tag{4}$$

where $\hat{\cdot}$ is the "hat map" that satisfies $\hat{\boldsymbol{a}}\boldsymbol{b} = \boldsymbol{a} \times \boldsymbol{b} \; \forall \; \boldsymbol{a}, \boldsymbol{b} \in \mathbb{R}^3$. As inputs, we have $\boldsymbol{u} = \begin{bmatrix} f^{\mathrm{T}} & \boldsymbol{\mu}^{\mathrm{T}} & \boldsymbol{\tau}^{\mathrm{T}} \end{bmatrix}^{\mathrm{T}} \in \mathbb{R}^6$, where $f \in \mathbb{R}$ is the thrust in the $\boldsymbol{R}_{OB}\boldsymbol{e}_3$ direction, $\boldsymbol{\mu} \in \mathbb{R}^3$ are the external moments about the axes of the floating base frame, and $\boldsymbol{\tau} \in \mathbb{R}^2$ are the joint torques generated by the arm motors.

As stated above, we will require S, the center of mass of the entire system, to be fixed in the end effector frame E. Explicitly, $\dot{\boldsymbol{p}}_{ES} = 0$. At first seeming restrictive, this requirement can be interpreted as a general design criterion, which may achieved by ensuring that the axis of rotation of each link is coincident with the combined center of mass of the previous links, starting from the floating base. For the class of aerial manipulators in 3D equipped with 2DOF arms, this requirement is analogous to the stipulation widely made in the planar aerial manipulator literature that the first link in the arm be attached at the center of mass of the floating base [8], [11], [15], however this is not sufficient in the full 3D case. This requirement will be necessary to demonstrate that the pose of the end effector is a valid *flat output* for the system, however it is not used in deriving the dynamic model. Also, experiments have shown that similar assumptions for planar aerial manipulators can serve as a useful approximation even in systems where they are not strictly satisfied [16].

III. Dynamics

Because we are interested in dynamic maneuvers, our system may experience conditions far from the static hover configuration. For this reason, it is not acceptable to introduce artificial singularities by deriving the dynamics using a chart on $\mathrm{SO}(3)$ (such as Euler angles) as generalized coordinates. We leverage a generalized Lagrangian method first presented in [27] and corrected and elaborated in [28]–[30] to derive coordinate- and singularity-free equations of motion directly on Q with $\boldsymbol{v} \in \mathbb{R}^8$ as our quasi-velocities. As in [30], we define a map $\boldsymbol{q} = \Phi(\boldsymbol{\varphi}; \boldsymbol{q}_0)$ that parametrizes the neighborhood of any element $\boldsymbol{q}_0 \in \mathrm{SE}(3) \times \mathbb{R}^2$ with local coordinates $\boldsymbol{\varphi} \in \mathbb{R}^8$. Correspondingly, we derive an invertible mapping $\boldsymbol{v} = \boldsymbol{S}(\boldsymbol{\varphi})\dot{\boldsymbol{\varphi}}$ that relates the variation in $\boldsymbol{\varphi}$ to the resulting element in our velocity space.

In this method, $\boldsymbol{q}_0$ is the origin of our local coordinate system with $\boldsymbol{\varphi}$ as our generalized coordinates. After completing the derivation of the dynamics using the local coordinates, the resulting expressions are evaluated at $\boldsymbol{\varphi} = 0$ (hence $\boldsymbol{q} = \boldsymbol{q}_0$) and the local velocities $\dot{\boldsymbol{\varphi}}$ are replaced by $\boldsymbol{v}$ using the invertible mapping, which will yield global singularity-free equations of motion in terms of the global coordinates $\{\boldsymbol{q}, \boldsymbol{v}\}$. For a more thorough explanation, the interested reader is directed to [30].

A. Local Maps

The local coordinate mapping is defined as

$$\Phi\left(\boldsymbol{\varphi};\boldsymbol{q}_0\right)=\left\{\boldsymbol{g}_{OB,0}\begin{bmatrix}\boldsymbol{R}_{\text{loc}}\left(\boldsymbol{\varphi}_{456}\right) & \boldsymbol{\varphi}_{123}\\ 0 & 1\end{bmatrix},\boldsymbol{\theta}_0+\boldsymbol{\varphi}_{78}\right\} \tag{5}$$

where we choose

$$\boldsymbol{R}_{\text{loc}}\left(\boldsymbol{\varphi}_{456}\right)=\exp(\varphi_4\hat{e}_1)\exp(\varphi_5\hat{e}_2)\exp(\varphi_6\hat{e}_3) \tag{6}$$

where we use the exponential map and the standard basis vectors $\boldsymbol{e}_i$. The velocity transformation $\boldsymbol{v}=\boldsymbol{S}\left(\boldsymbol{\varphi}\right)\dot{\boldsymbol{\varphi}}$ is derived by differentiating (5) and simplifying to yield

$$\boldsymbol{v}=\begin{bmatrix}\boldsymbol{R}_{\text{loc}}^{\mathrm{T}}\dot{\boldsymbol{\varphi}}_{123}\\ \left(\boldsymbol{R}_{\text{loc}}^{\mathrm{T}}\dot{\boldsymbol{R}}_{\text{loc}}\right)^{\vee}\\ \dot{\boldsymbol{\varphi}}_{78}\end{bmatrix} \tag{7}$$

where we make use again of the hat map and its inverse the "vee map", defined such that $\left(\hat{\boldsymbol{a}}\right)^{\vee}=\boldsymbol{a}$. Computing $\frac{\partial \boldsymbol{v}}{\partial \boldsymbol{\varphi}}$ from (7) will yield $\boldsymbol{S}(\boldsymbol{\varphi})$ since $\boldsymbol{v}$ is linear in $\dot{\boldsymbol{\varphi}}$.

B. Manipulator Equations

Using the results from [30], we will derive the coordinate-free dynamics in the form

$$\boldsymbol{M}(\boldsymbol{\theta})\dot{\boldsymbol{v}}+\boldsymbol{C}(\boldsymbol{\theta},\boldsymbol{v})\boldsymbol{v}+\boldsymbol{G}(\boldsymbol{q})=\boldsymbol{B}\boldsymbol{u} \tag{8}$$

Inertia Matrix, M: The inertia matrix is defined as

$$\boldsymbol{T}=\frac{1}{2}\boldsymbol{v}^{\mathrm{T}}\boldsymbol{M}\boldsymbol{v} \tag{9}$$

where $\boldsymbol{T}$ is the kinetic energy of the system. To start, we compute a geometric Jacobian for each body, such that

$$\boldsymbol{V}_{Oi}=\begin{bmatrix}\boldsymbol{v}_{Oi}\\ \boldsymbol{\omega}_{Oi}\end{bmatrix}=\boldsymbol{J}_i\boldsymbol{v} \tag{10}$$

where $\boldsymbol{V}_{Oi}$ is the twist of body i, represented in its local frame. We start with the translational velocity in the local frame expressed as the derivative of the global position.

$$\boldsymbol{v}_{Oi}=\boldsymbol{R}_{Oi}^{\mathrm{T}}\dot{\boldsymbol{p}}_{Oi} \tag{11}$$

Performing useful substitutions,

$$\boldsymbol{v}_{Oi}=\left(\boldsymbol{R}_{OB}\boldsymbol{R}_{Bi}\right)^{\mathrm{T}}\left(\dot{\boldsymbol{p}}_{OB}+\left(\boldsymbol{R}_{OB}\dot{\boldsymbol{p}}_{Bi}+\dot{\boldsymbol{R}}_{OB}\boldsymbol{p}_{Bi}\right)\right) \tag{12}$$

and simplifying yields

$$\boldsymbol{v}_{Oi}=\boldsymbol{R}_{Bi}^{\mathrm{T}}\left(\boldsymbol{v}_{OB}+\dot{\boldsymbol{p}}_{Bi}+\hat{\boldsymbol{\omega}}_{OB}\boldsymbol{p}_{Bi}\right) \tag{13}$$

where $\boldsymbol{p}_{Bi}$, $\dot{\boldsymbol{p}}_{Bi}$ can be directly computed from the transformation matrices between the bodies, which we do not define explicitly here for brevity. We now find the angular velocity of each rigid body relative to the spatial frame, expressed in its local frame by first noting that

$$\boldsymbol{R}_{Oi}=\boldsymbol{R}_{OB}\boldsymbol{R}_{Bi} \tag{14}$$

so that by using the same kinematics as (3), we obtain

$$\boldsymbol{\omega}_{Oi}=\left(\boldsymbol{R}_{Bi}^{\mathrm{T}}\hat{\boldsymbol{\omega}}_{OB}\boldsymbol{R}_{Bi}+\boldsymbol{R}_{Bi}^{\mathrm{T}}\dot{\boldsymbol{R}}_{Bi}\right)^{\vee} \tag{15}$$

We can now write

$$\boldsymbol{J}_i=\frac{\partial \boldsymbol{V}_{Oi}}{\partial \boldsymbol{v}} \tag{16}$$

Since (13) and (15) are linear in $\boldsymbol{v}$. Now, we consider the kinetic energy of each body as

$$\boldsymbol{T}_i=\frac{1}{2}\left(\boldsymbol{V}_{Oi}\right)^{\mathrm{T}}\mathcal{I}_i\boldsymbol{V}_{Oi} \tag{17}$$

Here, $\mathcal{I}_i$ is the 6×6 block diagonal inertia matrix

$$\mathcal{I}_i=\begin{bmatrix}m_i\boldsymbol{I}_3 & 0\\ 0 & \mathcal{J}_3\end{bmatrix} \tag{18}$$

where m_i and $\mathcal{J}_i$ are respectively the mass and moment of inertia tensor of body i and $\boldsymbol{I}_3$ is the identity. Then,

$$\boldsymbol{T}_i=\frac{1}{2}\boldsymbol{v}^{\mathrm{T}}\boldsymbol{J}_i^{\mathrm{T}}\mathcal{I}_i\boldsymbol{J}_i\boldsymbol{v} \tag{19}$$

and hence

$$\boldsymbol{M}=\sum_{i=\{b,1,2\}}\boldsymbol{J}_i^{\mathrm{T}}\mathcal{I}_i\boldsymbol{J}_i \tag{20}$$

Coriolis Matrix, C: The entries of the Coriolis matrix are given according to [30] as

$$\begin{aligned}C_{ij}=&\sum_{k=1}^{8}\left(\frac{\partial M_{ij}}{\partial\varphi_k}-\frac{1}{2}\frac{\partial M_{jk}}{\varphi_i}\right)\Big|_{\varphi=0}v_k\\&+\sum_{k=1}^{8}\sum_{s=1}^{8}\left(\frac{\partial S_{si}}{\partial\varphi_k}-\frac{\partial S_{sk}}{\partial\varphi_i}\right)M_{sj}\Big|_{\varphi=0}v_k\end{aligned} \tag{21}$$

Potential Field, G: The potential energy of the system due to gravity is

$$\boldsymbol{U}(\boldsymbol{q})=\sum_{i=\{b,1,2\}}m_i g\boldsymbol{e}_3^{\mathrm{T}}\boldsymbol{p}_{Oi} \tag{22}$$

The potential field is therefore given as [30]

$$\boldsymbol{G}=\boldsymbol{S}^{-\mathrm{T}}\left(\boldsymbol{\varphi}\right)\frac{\partial \boldsymbol{U}\left(\Phi\left(\boldsymbol{\varphi};\boldsymbol{q}_0\right)\right)}{\partial\boldsymbol{\varphi}}\Big|_{\varphi=0} \tag{23}$$

Input Matrix, B: The input matrix can be found through D'Alembert's principal, where we note that the virtual work done by applied forces is

$$\begin{aligned}\delta W&=\boldsymbol{u}^{\mathrm{T}}\boldsymbol{B}^{\mathrm{T}}\delta\boldsymbol{v}\\&=\boldsymbol{J}_u\delta\boldsymbol{v}\end{aligned} \tag{24}$$

We can derive $\boldsymbol{J}_u$ from the physical structure of our system as

$$\begin{aligned}\boldsymbol{J}_u=&\boldsymbol{\mu}^{\mathrm{T}}\boldsymbol{J}_{B,\omega}+f\boldsymbol{e}_3^{\mathrm{T}}\boldsymbol{J}_{B,v}+\tau_1\boldsymbol{e}_1^{\mathrm{T}}\left(\boldsymbol{J}_{1,\omega}-\boldsymbol{J}_{B,\omega}\right)\\&+\tau_2\left(\boldsymbol{e}_2^{\mathrm{T}}\boldsymbol{J}_{2,\omega}-\boldsymbol{e}_2^{\mathrm{T}}\boldsymbol{R}_{12}^{\mathrm{T}}\boldsymbol{J}_{1,\omega}\right)\end{aligned} \tag{25}$$

where $\boldsymbol{v}_{Oi}=\boldsymbol{J}_{i,\boldsymbol{v}}\boldsymbol{v}$ and $\boldsymbol{\omega}_{Oi}=\boldsymbol{J}_{i,\boldsymbol{\omega}}\boldsymbol{v}$, and because (25) is linear in $\boldsymbol{u}$,

$$\boldsymbol{B}=\left(\frac{\partial \boldsymbol{J}_u}{\partial \boldsymbol{u}}\right)^{\mathrm{T}}=\begin{bmatrix}0_{2\times 6}\\ \boldsymbol{I}_6\end{bmatrix} \tag{26}$$

This result is expected, since the inputs $\boldsymbol{u}$ can be described as *collocated* with a subset of $\boldsymbol{v}$ [31]. We now have an explicit, coordinate-free, singularity-free representation of the dynamics. It can also be shown that the matrices have the state dependencies noted in (8).

IV. Inertial Decomposition

In this section, we transform the dynamic equations derived in the last section into a form that allows us to decompose and analyze the fundamental subsystems of the aerial manipulator. We will find a representation of the system's dynamics in a similar form to (8) but with a block-diagonal inertia matrix and a separation of the underactuated and fully actuated cascaded physical subsystems. Using principles related to early work in with spacecraft-manipulators [32], we utilize the inertial decoupling technique presented in [18], with the transformed configuration and velocity coordinates

$$\boldsymbol{\Xi} := \begin{bmatrix} \boldsymbol{x}_S \\ \boldsymbol{R}_{OB} \\ \boldsymbol{\theta} \end{bmatrix}, \quad \boldsymbol{\xi} := \begin{bmatrix} \dot{\boldsymbol{x}}_S \\ \boldsymbol{\omega}_{OB} \\ \boldsymbol{\rho} \end{bmatrix} \tag{27}$$

where $\boldsymbol{x}_S$ is the position of the system center of mass in the inertial frame O and $\boldsymbol{\rho}$ is a generalized manipulator velocity that is independent of $\boldsymbol{x}_S$ and $\boldsymbol{\omega}_{OB}$. Drawing from [18], we relate the standard and decoupled velocities by the transformation

$$\boldsymbol{\xi} = \boldsymbol{T}\boldsymbol{v} := \begin{bmatrix} \boldsymbol{T}_S \\ \boldsymbol{T}_\omega \\ \boldsymbol{T}_\rho \end{bmatrix} \boldsymbol{v} \tag{28}$$

where $\boldsymbol{T}_S$ and $\boldsymbol{T}_\omega$ are simply the Jacobians of the system center of mass velocity $\dot{\boldsymbol{x}}_S$ and the floating base angular velocity $\boldsymbol{\omega}_{OB}$ respectively, and we must still determine $\boldsymbol{T}_\rho$. To satisfy the block diagonality criterion, it must hold for each pair of inertially decoupled velocity elements

$$\boldsymbol{T}_\alpha \boldsymbol{M}^{-1} \boldsymbol{T}_\beta^{\mathrm{T}} = \boldsymbol{0}, \ \alpha, \beta \in \{S, \omega, \rho\}, \alpha \neq \beta \tag{29}$$

$\boldsymbol{T}_\rho$ can therefore derived as a dynamically consistent nullspace projector as shown in [18] which will achieve this property. To find $\boldsymbol{T}_\rho$, we first compute

$$\boldsymbol{Z} = \mathrm{N}\left(\begin{bmatrix} \boldsymbol{T}_S & \boldsymbol{T}_\omega \end{bmatrix}\right)^{\mathrm{T}} \tag{30}$$

where $\mathrm{N}(\cdot)$ is the nullspace operator. Then the result is

$$\boldsymbol{T}_\rho = (\boldsymbol{Z}\boldsymbol{M}\boldsymbol{Z}^{\mathrm{T}})^{-1}\boldsymbol{Z}\boldsymbol{M} \tag{31}$$

The use of the system center of mass as a decoupling transformation has been utilized widely in the analysis of aerial manipulators, and it is physically understood that $\dot{\boldsymbol{x}}_S$ and $\boldsymbol{\omega}_{OB}$ will be inertially decoupled since $\ddot{\boldsymbol{x}}_S$ depends only on the net external force, and the inertia matrix with any set of generalized velocities must be positive definite. This is easily verified by (29).

Having found $\boldsymbol{T}$, we can now decouple the system by premultiplying (8) by $\boldsymbol{T}^{-\mathrm{T}}$ and performing substitutions for $\boldsymbol{v}, \dot{\boldsymbol{v}}$, giving the inertially decoupled dynamics

$$\boldsymbol{\Lambda}\dot{\boldsymbol{\xi}} + \boldsymbol{\Gamma}\xi + \mathcal{N} = \mathcal{B}\boldsymbol{u} \tag{32}$$

Expanding the above dynamics for each inertially decoupled subsystem using submatrices from above, we have

$$S_1 := \quad m\ddot{\boldsymbol{x}}_S + mg\boldsymbol{e}_3 = f\boldsymbol{R}_{OB}\boldsymbol{e}_3 \tag{33}$$

$$S_2 := \quad \boldsymbol{\Lambda}_2\dot{\boldsymbol{\omega}}_{OB} + \boldsymbol{\Gamma}_2\xi = \mathcal{B}_2\boldsymbol{u} \tag{34}$$

$$S_3 := \quad \boldsymbol{\Lambda}_3\dot{\boldsymbol{\rho}} + \boldsymbol{\Gamma}_3\xi = \mathcal{B}_3\boldsymbol{u} \tag{35}$$

where m is the total mass of the system. Note that the transformed Coriolis matrix $\boldsymbol{\Gamma}$ does not affect the center of mass dynamics, and the potential field $\mathcal{N}$ only affects the center of mass dynamics. The composition of S_1 and S_2 is nearly equivalent to the standard quadrotor, the notable difference being the velocity coupling with the other subsystems.

V. Differential Flatness

In this section, we will demonstrate that the system is differentially flat, allowing us to plan dynamically feasible trajectories for the system in an unconstrained flat space. A system with state $\mathcal{X}$ and input $\mathcal{U}$ is differentially flat with respect to some *flat output* $\mathcal{Y}$ if there exists a diffeomorpism between $\mathbf{y} = (\mathcal{Y}, \dot{\mathcal{Y}}, ..., \mathcal{Y}^{(p)})$ and the extended state $\mathbf{x} = (\mathcal{X}, \mathcal{U}, \dot{\mathcal{U}}, ..., \mathcal{U}^{(n)})$ [33]. In other words, we must find smooth algebraic functions determining $\mathbf{x}$ as a function of $\mathbf{y}$, and likewise $\mathbf{y}$ as a function of $\mathbf{x}$. With this diffeomorphism, given any sufficiently smooth trajectory $\mathcal{Y}(t)$ in the flat space, we can determine the necessary inputs $\mathcal{U}(t)$ to track the flat space trajectory and the corresponding system states $\mathcal{X}(t)$.

We propose the flat output

$$\mathcal{Y} := \boldsymbol{g}_{OE} = \begin{bmatrix} \boldsymbol{R}_{OE} & \boldsymbol{p}_{OE} \\ 0 & 1 \end{bmatrix} \tag{36}$$

so that we will be able plan physically useful trajectories via the pose of the end effector frame E. Note that to strictly satisfy the classical definition of flatness, the flat space must be $\mathbb{R}^n$ such that the dynamics are transformed into a linear system. Here we make a mild abuse of the terminology, but note that *any* chart on SO(3) injected into our analysis would automatically provide a choice of flat outputs that strictly satisfies the classical definition.

A. Constraints Arising From Underactuation

In this section, we will state certain kinematic constraints on the floating base that must be satisfied by the system's trajectory due its underactuation. These equations are derived in detail in [34] for the standard quadrotor. Thanks to the near-equivalence of the standard quadrotor and the combination of subsystems S_1 and S_2 of our system, we obtain identical kinematic requirements on the floating base. Note that here we employ the shorthand

$$\begin{bmatrix} \omega_1 \\ \omega_2 \\ \omega_3 \end{bmatrix} := \boldsymbol{\omega}_{OB}, \ \begin{bmatrix} \boldsymbol{b}_1 & \boldsymbol{b}_2 & \boldsymbol{b}_3 \end{bmatrix} := \boldsymbol{R}_{OB} \tag{37}$$

First, we note that we can find directly from the flat output $\boldsymbol{g}_{OE}$ the corresponding system center of mass trajectory

$$\boldsymbol{x}_S = \boldsymbol{g}_{OE}\boldsymbol{p}_{ES} \tag{38}$$

where p_{ES} denotes the location of S in E, and successive derivatives of $\boldsymbol{x}_S$ can be found by direct differentiation of (38). We note that from (33) that the thrust vector must be in the direction of the combined gravity and acceleration vector.

$$f\boldsymbol{b}_3 = m\left(\ddot{\boldsymbol{x}}_S + g\boldsymbol{e}_3\right) \tag{39}$$

Hence we see that

$$f = m \left\| \ddot{\boldsymbol{x}}_S + g\boldsymbol{e}_3 \right\|_2 \tag{40}$$

and projection of the derivative of (39) onto $\boldsymbol{b}_3$ will also show that

$$\dot{f} = m\boldsymbol{b}_3^{\mathrm{T}} \boldsymbol{x}_S^{(3)} \tag{41}$$

Differentiating (39) twice and solving for the components of interest will reveal additional constraints on the angular velocity and angular acceleration of the floating base in the form

$$\begin{bmatrix} \omega_1 \\ \omega_2 \end{bmatrix} = \frac{m}{f} \begin{bmatrix} -\boldsymbol{b}_2^{\mathrm{T}} \\ \boldsymbol{b}_1^{\mathrm{T}} \end{bmatrix} \boldsymbol{x}_S^{(3)} \tag{42}$$

$$\begin{bmatrix} \dot{\omega}_1 \\ \dot{\omega}_2 \end{bmatrix} = \frac{m}{f} \begin{bmatrix} -\boldsymbol{b}_2^{\mathrm{T}} \\ \boldsymbol{b}_1^{\mathrm{T}} \end{bmatrix} \boldsymbol{x}_S^{(4)} - 2\frac{\dot{f}}{f} \begin{bmatrix} \omega_1 \\ \omega_2 \end{bmatrix} + \omega_3 \begin{bmatrix} \omega_2 \\ -\omega_1 \end{bmatrix} \tag{43}$$

B. State Trajectories

Using the previous constraints, we can determine the necessary trajectories for the state variables to achieve the prescribed end effector trajectory.[1] Rearranging (39),

$$f\boldsymbol{R}_{12}^{\mathrm{T}}\boldsymbol{R}_{B1}^{\mathrm{T}}\boldsymbol{e}_3 = m\boldsymbol{R}_{OE}^{\mathrm{T}}\left(\ddot{\boldsymbol{x}}_S + g\boldsymbol{e}_3\right) \tag{44}$$

and defining for brevity

$$\boldsymbol{z} := \frac{m}{f}\boldsymbol{R}_{OE}^{\mathrm{T}}\left(\ddot{\boldsymbol{x}}_S + g\boldsymbol{e}_3\right) \tag{45}$$

we expand the left-hand side of (44), giving

$$\begin{bmatrix} -\cos\theta_1 \sin\theta_2 \\ \sin\theta_1 \\ \cos\theta_1 \cos\theta_2 \end{bmatrix} = \boldsymbol{z} \tag{46}$$

allowing us to determine the joint angles $\boldsymbol{\theta}$ as[2]

$$\theta_2 = \operatorname{atan2}\left(-z_1, z_3\right) \tag{47}$$

$$\theta_1 = \operatorname{atan2}\left(z_2 \sin\theta_2, -z_1\right) \tag{48}$$

To determine the joint velocities $\dot{\boldsymbol{\theta}}$, we rearrange the forward kinematics of the manipulator

$$\boldsymbol{R}_{OB} = \boldsymbol{R}_{OE}\left(\boldsymbol{R}_{B1}\boldsymbol{R}_{12}\right)^{\mathrm{T}} \tag{49}$$

and differentiate, also using (3), to determine

$$\boldsymbol{\omega}_{OB} = \left(\boldsymbol{R}_{B1}\dot{\boldsymbol{R}}_{B1}^{\mathrm{T}} + \boldsymbol{R}_{B2}\dot{\boldsymbol{R}}_{12}^{\mathrm{T}}\boldsymbol{R}_{B1}^{\mathrm{T}} + \boldsymbol{R}_{B2}\hat{\boldsymbol{\omega}}_{OE}\boldsymbol{R}_{B2}^{\mathrm{T}}\right)^{\vee} \tag{50}$$

where we note that $\boldsymbol{R}_{OE}$ cancels out. We can rewrite (50) in explicitly linear form as

$$\boldsymbol{\omega}_{OB} = \boldsymbol{A}_\omega\boldsymbol{\omega}_{OE} + \boldsymbol{A}_\theta\dot{\boldsymbol{\theta}} \tag{51}$$

where $\boldsymbol{A}_\omega, \boldsymbol{A}_\theta$ depend only on $\boldsymbol{\theta}$. Expanding the first two rows and solving for $\dot{\boldsymbol{\theta}}$, we have[3]

$$\dot{\boldsymbol{\theta}} = \begin{bmatrix} 1 & 0 \\ 0 & \frac{1}{\cos\theta_1} \end{bmatrix} \left(\begin{bmatrix} \boldsymbol{e}_1^{\mathrm{T}} \\ \boldsymbol{e}_2^{\mathrm{T}} \end{bmatrix} \boldsymbol{A}_\omega\boldsymbol{\omega}_{OE} - \begin{bmatrix} \omega_1 \\ \omega_2 \end{bmatrix} \right) \tag{52}$$

To find $\ddot{\boldsymbol{\theta}}$, we take the derivative of (51)

$$\dot{\boldsymbol{\omega}}_{OB} = \dot{\boldsymbol{A}}_\omega\boldsymbol{\omega}_{OE} + \boldsymbol{A}_\omega\dot{\boldsymbol{\omega}}_{OE} + \dot{\boldsymbol{A}}_\theta\dot{\boldsymbol{\theta}} + \boldsymbol{A}_\theta\ddot{\boldsymbol{\theta}} \tag{53}$$

and solve for $\ddot{\boldsymbol{\theta}}$, giving

$$\begin{aligned} \ddot{\boldsymbol{\theta}} = \begin{bmatrix} 1 & 0 \\ 0 & \frac{1}{\cos\theta_1} \end{bmatrix} \Bigg(& - \begin{bmatrix} \dot{\omega}_1 \\ \dot{\omega}_2 \end{bmatrix} \\ & + \begin{bmatrix} \boldsymbol{e}_1^{\mathrm{T}} \\ \boldsymbol{e}_2^{\mathrm{T}} \end{bmatrix} \left(\dot{\boldsymbol{A}}_\omega\boldsymbol{\omega}_{OE} + \boldsymbol{A}_\omega\dot{\boldsymbol{\omega}}_{OE} + \dot{\boldsymbol{A}}_\theta\dot{\boldsymbol{\theta}} \right) \Bigg) \end{aligned} \tag{54}$$

By substituting into (47), (48), (52), and (54) the results above for $\omega_1, \omega_2, \dot{\omega}_1, \dot{\omega}_2$, and $\boldsymbol{b}_3$ in terms of the flat outputs, $\boldsymbol{\theta}, \dot{\boldsymbol{\theta}}$, and $\ddot{\boldsymbol{\theta}}$ are fully determined.

Note that after solving for $\boldsymbol{\theta}$ in (47) and (48), $\boldsymbol{R}_{OB}$ can be determined from (49). Additionally, the solutions for $\dot{\boldsymbol{\theta}}$, $\ddot{\boldsymbol{\theta}}$ from (52) and (54), will provide ω_3 and $\dot{\omega}_3$ from (51) and (53) respectively. Finally, $\dot{\boldsymbol{\rho}}$ can be determined directly from

$$\dot{\boldsymbol{\xi}} = \dot{\boldsymbol{T}}\boldsymbol{v} + \boldsymbol{T}\dot{\boldsymbol{v}} \tag{55}$$

C. Computing Inputs

Now, using the transformed dynamics in (33)-(35), we can determine the necessary inputs to track the trajectory. f was already determined above for convenience in the derivation. It is then straightforward to compute

$$\begin{bmatrix} \boldsymbol{\mu} \\ \boldsymbol{\tau} \end{bmatrix} = \mathcal{B}_{\mu\boldsymbol{\tau}}^{-1} \left(\begin{bmatrix} \boldsymbol{\Lambda}_2 & 0 \\ 0 & \boldsymbol{\Lambda}_3 \end{bmatrix} \begin{bmatrix} \dot{\boldsymbol{\omega}}_{OB} \\ \dot{\boldsymbol{\rho}} \end{bmatrix} + \begin{bmatrix} \boldsymbol{\Gamma}_2 \\ \boldsymbol{\Gamma}_3 \end{bmatrix} \xi - f\mathcal{B}_f \right) \tag{56}$$

where we use the notation

$$\begin{bmatrix} \mathcal{B}_2 \\ \mathcal{B}_3 \end{bmatrix} = \begin{bmatrix} \mathcal{B}_f & \mathcal{B}_{\mu\boldsymbol{\tau}} \end{bmatrix} \tag{57}$$

Intuitively we know that $\mathcal{B}_{\mu\boldsymbol{\tau}}$ will be invertible because the S_1 and S_2 subsystems are fully actuated, but in fact it can be shown that it is upper triangular and full rank.

The inverse diffeomorphism is trivial since it is simply the system's forward kinematics. The fourth derivatives of the flat outputs appear in the equations, hence for any $\boldsymbol{g}_{OE}(t) \in \mathcal{C}^4$ satisfying self-collision constraints, we can determine the necessary inputs $\boldsymbol{u}(t)$ to permit the end effector to track exactly that trajectory, as well as the transformed system state $\{\boldsymbol{\Xi}(t), \boldsymbol{\xi}(t)\}$ corresponding to that trajectory in the flat space. It is straightforward to then transform back to the original representation $\{\boldsymbol{q}(t), \boldsymbol{v}(t)\}$ using the results already given.

In addition to planning dynamically feasible trajectories and solving for nominal inputs, the application of this approach to a physical system would require a closed loop

[1] For comprehensibility, we analyze here the particular geometry of Fig. 1, but this approach can be used for any geometry satisfying the center of mass assumption discussed previously.

[2] The relationships (47), (48) hold on the domain $\boldsymbol{\theta} \in \left(-\frac{\pi}{2}, \frac{\pi}{2}\right) \times (0, \pi)$, the self-collision-free workspace of the system.

[3] Note that $\theta_1 = \pm\frac{\pi}{2}$ corresponds to the physical singularity when the axis of θ_2 is parallel to the $\boldsymbol{b}_3$ axis, which causes a loss of full manipulability due to the physical structure of the system. However, in practical circumstances self-collision would prevent this configuration from ever occuring.

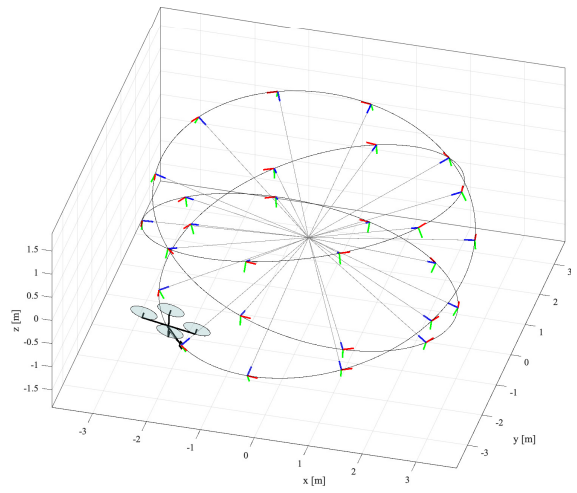

Fig. 2: The system tracks a 6DOF end effector trajectory in simulation to achieve a precision aerial videography task.

controller. This is not addressed in detail here due to space constraints. However, because of the similarity of the composition of S_1 and S_2 to the standard quadrotor, it is possible to adapt well-known controllers from the literature [35] to the transformed subsystems by canceling the velocity couplings in the S_2 system, which is possible due to S_2 being fully actuated. Since S_3 is also fully actuated, feedback linearization can provide a straightforward controller for the arm subsystem. The cascaded configuration of the rotational and translational subsystems indicates backstepping control design as an obvious choice to stabilize the system [33].

VI. Simulation

MATLAB's symbolic manipulation toolbox was used to derive the system dynamics and perform the inertial decomposition according to the steps described in Sec. III and IV. The diffeomorphism presented in Sec. V was implemented to verify its correctness for the dynamic model derived. To demonstrate the usefulness of being able to prescribe an arbitrary smooth trajectory for the end effector pose, we turn to aerial videography, a field that MAVs have dramatically expanded in recent years. A videographer may wish to capture a shot that dramatically varies the perspective while precisely maintaining a subject centered in the field of view and keeping the horizon line flat in the shot, a task for which an aerial manipulator is ideally suited. Fig. 2 demonstrates such a trajectory orbiting a subject, specified in the flat space. Using the proposed approach, we are able to compute the system's state trajectory and input profile corresponding to the prescribed trajectory $g_{OE}(t)$ in the flat space shown respectively in Fig. 3 and Fig. 4. We simulate applying these inputs to the system completely open-loop with no stabilizing controller, and demonstrate that the end effector tracks the desired trajectory with translational and angular RMSE of $3.3 \times 10^{-8}\,\mathrm{m}$ and $2.7 \times 10^{-5}\,\mathrm{rad}$ over a $15\,\mathrm{s}$ trajectory, which is consistent with the expected numerical error from integrating the system's nonlinear dynamics. The simulation is presented in further detail in the accompanying video. [4]

VII. Conclusion

This paper derived a coordinate-free dynamic model for a class of 3D aerial manipulators, avoiding the artificial singularities introduced by most prior work and accounting for the inertia of all three coupled rigid bodies. Using this model and an inertial decoupling transformation, the system was demonstrated to be differentially flat with respect to the end effector pose, allowing us to track an arbitrary any physically realizable task-space trajectory in 6DOF. For this task, the proposed system is minimal in the number of inputs as the dimension of the flat output manifold and input vector is 6. Exciting future opportunities include the implementation of the planning approach on a physical platform for the completion of real-world manipulation tasks, and a more general formulation for an n-link manipulator. Additionally, while the derivation of the dynamics is not limited to the case where the system center of mass is fixed in the end effector frame, the flatness argument relies on this to achieve a closed form solution. In the general case, (44) results in a system of nonlinear ODEs that cannot be solved analytically. However, it may be possible to incorporate these as constraints in a nonlinear optimization-based planner, suggesting the applicability of some of these ideas in cases where the center of mass criterion required here is not realistic.

Acknowledgements

The first author gratefully acknowledges the invaluable mentorship of Dr. Justin Thomas, a GRASP alumnus.

[4] Available in higher quality at `www.jakewelde.com/icra2020`.

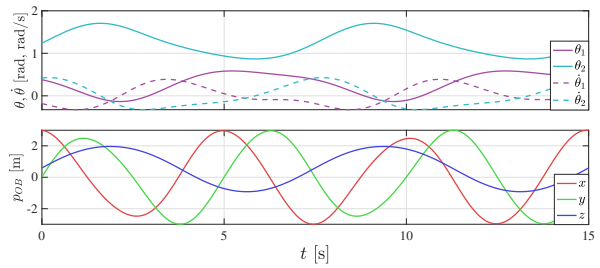

Fig. 3: A portion of the state trajectory computed from the end effector trajectory in the flat space depicted in Fig. 2.

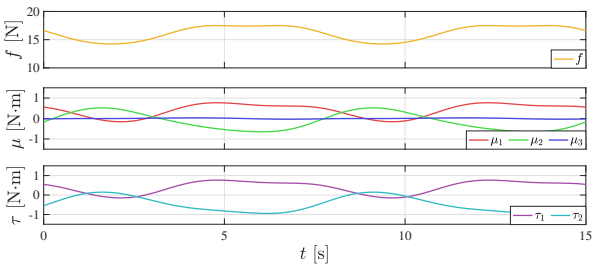

Fig. 4: Input profile necessary to achieve the end effector trajectory in the flat space depicted in Fig. 2.

REFERENCES

[1] C. Zhang and J. M. Kovacs, "The application of small unmanned aerial systems for precision agriculture: A review," *Precision Agriculture*, vol. 13, no. 6, pp. 693–712, 2012.

[2] M. Erdelj, E. Natalizio, K. R. Chowdhury, and I. F. Akyildiz, "Help from the Sky: Leveraging UAVs for Disaster Management," *IEEE Pervasive Computing*, vol. 16, no. 1, pp. 24–32, 2017.

[3] C. A. Thiels, J. M. Aho, S. P. Zietlow, and D. H. Jenkins, "Use of unmanned aerial vehicles for medical product transport," *Air Medical Journal*, vol. 34, no. 2, pp. 104–108, 2015. [Online]. Available: http://dx.doi.org/10.1016/j.amj.2014.10.011

[4] M. A. Garcia, R. A. Rojas, and F. Pirri, "Object-centered teleoperation of mobile manipulators with remote center of motion constraint," *IEEE Robotics and Automation Letters*, vol. 4, no. 2, pp. 1745–1752, 2019.

[5] A. Specian, C. Mucchiani, M. Yim, and J. Seo, "Robotic edge-rolling manipulation: A grasp planning approach," *IEEE Robotics and Automation Letters*, vol. 3, no. 4, pp. 3137–3144, 2018.

[6] M. Kennedy, K. Schmeckpeper, D. Thakur, C. Jiang, V. Kumar, and K. Daniilidis, "Autonomous Precision Pouring from Unknown Containers," *IEEE Robotics and Automation Letters*, vol. 4, no. 3, pp. 2317–2324, 2019.

[7] C. H. Corbato, M. Bharatheesha, J. Van Egmond, J. Ju, and M. Wisse, "Integrating different levels of automation: Lessons from winning the amazon robotics challenge 2016," *IEEE Transactions on Industrial Informatics*, vol. 14, no. 11, pp. 4916–4926, 2018.

[8] M. Tognon, Y. Burak, G. Buondonno, A. Franchi, M. Tognon, Y. Burak, G. Buondonno, A. Franchi, E. Computations, and B. Antonio, "Explicit Computations , Simulations and additional Results for the Dynamic Decentralized Control for Protocentric Aerial Manipulators To cite this version : Explicit Computations , Simulations and additional Results for the Dynamic Decentralized Control f," in *IEEE International Conference on Robotics and Automation*, 2017.

[9] F. Ruggiero, V. Lippiello, and A. Ollero, "Aerial manipulation: A literature review," *IEEE Robotics and Automation Letters*, vol. 3, no. 3, pp. 1957–1964, 2018.

[10] M. Ryll, G. Muscio, F. Pierri, E. Cataldi, G. Antonelli, F. Caccavale, and A. Franchi, "6D physical interaction with a fully actuated aerial robot," *Proceedings - IEEE International Conference on Robotics and Automation*, pp. 5190–5195, 2017.

[11] J. Thomas, J. Polin, K. Sreenath, and V. Kumar, "Avian-inspired grasping for quadrotor Micro UAVs," in *Proceedings of the ASME Design Engineering Technical Conference*, vol. 6 A, 2013.

[12] P. Kotaru, G. Wu, and K. Sreenath, "Differential-flatness and control of quadrotor(s) with a payload suspended through flexible cable(s)," *2018 Indian Control Conference, ICC 2018 - Proceedings*, vol. 2018-Janua, pp. 352–357, 2018.

[13] S. Tang and V. Kumar, "Mixed Integer Quadratic Program trajectory generation for a quadrotor with a cable-suspended payload," *Proceedings - IEEE International Conference on Robotics and Automation*, vol. 2015-June, no. June, pp. 2216–2222, 2015.

[14] Y. Yu and V. Lippiello, "6D pose task trajectory tracking for a class of 3D aerial manipulator from differential flatness," *IEEE Access*, vol. 7, pp. 52 257–52 265, 2019.

[15] B. Yüksel, G. Buondonno, and A. Franchi, "Differential flatness and control of protocentric aerial manipulators with any number of arms and mixed rigid-/elastic-joints," *IEEE International Conference on Intelligent Robots and Systems*, vol. 2016-Novem, pp. 561–566, 2016.

[16] M. Tognon, B. Yuksel, G. Buondonno, and A. Franchi, "Dynamic decentralized control for protocentric aerial manipulators," *Proceedings - IEEE International Conference on Robotics and Automation*, pp. 6375–6380, 2017.

[17] H. Yang and D. Lee, "Dynamics and control of quadrotor with robotic manipulator," *Proceedings - IEEE International Conference on Robotics and Automation*, pp. 5544–5549, 2014.

[18] G. Garofalo, F. Beck, and C. Ott, "Task-space Tracking Control for Underactuated Aerial Manipulators," *2018 European Control Conference, ECC 2018*, pp. 628–634, 2018.

[19] P. O. Pereira, R. Zanella, and D. V. Dimarogonas, "Decoupled design of controllers for aerial manipulation with quadrotors," *IEEE International Conference on Intelligent Robots and Systems*, vol. 2016-Novem, no. 644128, pp. 4849–4855, 2016.

[20] A. Suarez, G. Heredia, and A. Ollero, "Lightweight compliant arm with compliant finger for aerial manipulation and inspection," *IEEE International Conference on Intelligent Robots and Systems*, vol. 2016-Novem, pp. 4449–4454, 2016.

[21] G. Arleo, F. Caccavale, G. Muscio, and F. Pierri, "Control of quadrotor aerial vehicles equipped with a robotic arm," *2013 21st Mediterranean Conference on Control and Automation, MED 2013 - Conference Proceedings*, pp. 1174–1180, 2013.

[22] V. Lippiello and F. Ruggiero, *Cartesian impedance control of a UAV with a robotic Arm*. IFAC, 2012, vol. 10, no. PART 1. [Online]. Available: http://dx.doi.org/10.3182/20120905-3-HR-2030.00158

[23] A. E. Jimenez-Cano, J. Martin, G. Heredia, A. Ollero, and R. Cano, "Control of an aerial robot with multi-link arm for assembly tasks," *Proceedings - IEEE International Conference on Robotics and Automation*, pp. 4916–4921, 2013.

[24] G. Heredia, A. E. Jimenez-Cano, I. Sanchez, D. Llorente, V. Vega, J. Braga, J. A. Acosta, and A. Ollero, "Control of a multirotor outdoor aerial manipulator," *IEEE International Conference on Intelligent Robots and Systems*, no. Iros, pp. 3417–3422, 2014.

[25] M. J. Kim, K. Kondak, and C. Ott, "A Stabilizing Controller for Regulation of UAV with Manipulator," *IEEE Robotics and Automation Letters*, vol. 3, no. 3, pp. 1719–1726, 2018.

[26] P. O. Pereira and D. V. Dimarogonas, "Pose and position trajectory tracking for aerial transportation ofa rod-like object," *Automatica*, vol. 109, p. 108547, 2019. [Online]. Available: https://doi.org/10.1016/j.automatica.2019.108547

[27] V. Duindam and S. Stramigioli, "Lagrangian dynamics of open multibody systems with generalized holonomic and nonholonomie joints," *IEEE International Conference on Intelligent Robots and Systems*, no. 1, pp. 3342–3347, 2007.

[28] P. J. From, V. Duindam, and S. Stramigioli, "Corrections to singularity-free dynamic equations of open-chain mechanisms with general holonomic and nonholonomic joints," *IEEE Transactions on Robotics*, vol. 28, no. 6, pp. 1431–1432, 2012.

[29] P. J. From, "An Explicit Formulation of Singularity-Free Dynamic Equations of Mechanical Systems in Lagrangian Form- Part One: Single Rigid Bodies," *Modeling, Identification and Control*, vol. 33, no. 2, pp. 61–68, 2012.

[30] ——, "An Explicit Formulation of Singularity-Free Dynamic Equations of Mechanical Systems in Lagrangian Form- Part Two: Multibody Systems," *Modeling, Identification and Control*, vol. 33, no. 2, pp. 61–68, 2012.

[31] J. T. Gravdahl, P. J. From, and K. Y. Pettersen, *Vehicle-Manipulator Systems - Modeling for Simulation, Analysis, and Control*. Springer, 2014.

[32] Z. Vafa and S. Dubowsky, "On the Dynamics of Manipulators in Space Using the Virtual Manipulator Approach," *Proceedings - IEEE International Conference on Robotics and Automation*, pp. 579–585, 1987.

[33] A. Drouin, S. S. Cunha, A. C. Brandao Ramos, and F. Mora-Camino, "Differential flatness and control of nonlinear systems," *Proceedings of the 30th Chinese Control Conference, CCC 2011*, no. 8, pp. 643–648, 2011.

[34] J. Thomas, "Grasping, Perching, and Visual Servoing for Micro Aerial Vehicles," Ph.D. dissertation, University of Pennsylvania, 2017.

[35] D. Mellinger and V. Kumar, "Minimum snap trajectory generation and control for quadrotors," *Proceedings - IEEE International Conference on Robotics and Automation*, pp. 2520–2525, 2011.